Fast Sizing Procedure for Salient-Pole Wound Field Synchronous Motors for Transportation Electrification

# Fast Sizing Procedure for Salient-Pole Wound Field Synchronous Motors for Transportation Electrification

Federica Graffeo, *Student Member, IEEE*
*Politecnico di Torino*
*Dipartimento di Energia*
Turin, Italy
federica.graffeo@polito.it

Silvio Vaschetto, *Senior Member, IEEE*
*Politecnico di Torino*
*Dipartimento di Energia*
Turin, Italy
silvio.vaschetto@polito.it

Alberto Tenconi, *Senior Member, IEEE*
*Politecnico di Torino*
*Dipartimento di Energia*
Turin, Italy
alberto.tenconi@polito.it

Andrea Cavagnino, *Fellow, IEEE*
*Politecnico di Torino*
*Dipartimento di Energia*
Turin, Italy
andrea.cavagnino@polito.it

***Abstract*— This paper presents an electromagnetic sizing procedure for the preliminary design of wound field synchronous motors for traction applications. The rated data, the permissible electromagnetic loadings, and few initial geometry and winding specifications are requested as input for the algorithm. The procedure is based on an analytical-numerical approach, consisting of increasing the machine rotor diameter until the requested performances are obtained respecting all the imposed constraints. A preliminary lamination geometry is built only using analytical equations and considering the no-load operating conditions of the machine. The sizing procedure is therefore completed at rated load using finite element simulations. In this paper, the proposed procedure is validated on a highly engineered wound field synchronous motor used for transportation applications.**

***Keywords*— *wound field synchronous machines, externally excited synchronous machines, separately excited synchronous machines, electromagnetic sizing.***

## I. INTRODUCTION

The permanent magnet synchronous motors and the induction motors are currently the most popular types of electric machine used by automotive original equipment manufacturers. However, there has been a recent interest in wound field synchronous motors (WFSMs) as an alternative technology for traction applications [1]-[4]. This machine type, also known as externally excited or separately excited synchronous motor, hosts a winding in the rotor that allows creating the excitation field without the use of permanent magnets, thus avoiding the risk of demagnetization or uncontrolled generations. Moreover, a constant power for a wide speed range can be accomplished thanks to the possibility of completely controlling the field excitation, and optimal field weakening operations with loss minimization can be achieved over the whole driving cycle. Also, being able to control both the stator and rotor current, high values of the power factor can be obtained, reducing the inverter size [5].

So far, the reason for the low popularity of WFSMs as propulsion motor is the necessity to bring current to the rotor, a task generally accomplished by brushes and slip rings. However, unlike the commutators of DC machines, the brushes and slip rings of WFSMs are supplied with relatively low *dc* power, making their wearing compatible with the requirements of transportation applications. Moreover, various technologies, such as harmonic, capacitive, and inductive power transfers, can be used as potential wireless substitutes to transfer the excitation current to the rotor [6].

However, because of the additional degree of freedom offered by the rotor current, the electromagnetic design of WFSMs might not be straightforward. Although many theoretical and empirical formulations are available in the literature for the design of large alternators for power plant applications, the challenging performance dictated by the transportation applications often leads to the necessity to exploit the design solutions of WFSMs up their maximum levels.

For example, the most recent technical literature reports different design methodologies for WFSMs that are mainly based on computational algorithms or optimization procedures. While the former usually refine recursively the machine geometry to achieve the design specifications, the latter explore a large design space to find the best machine candidate [7]-[11]. These methodologies generally exploit different approaches to identify the machine design solution: (i) analytical formulations, (ii) Finite Element Method (FEM) simulations, or (iii) Magnetic Equivalent Circuits (MEC). Optimizations based on FEM simulations usually achieve the best design solution with the most accurate results [6]. However, the computational burden required by FEM approach makes it unpopular for fast evaluations aimed to technical discussion or for initial cost evaluations. On the other hand, computational algorithms based on analytical formulations are the fastest in solving, but generally need FEM or MEC analyses to confirm the results accuracy [12].

In the present paper, the authors propose a preliminary, but still accurate, fast sizing procedure for salient pole wound field synchronous motors. The methodology consists of a mixed analytical-numerical approach to trade-off the fast computation time of the analytical formulations with accurate FEM analyses. In detail, the sizing procedure progressively increases the machine diameter until all the input constraints are respected, and the rated performances guaranteed. The preliminary lamination geometry is obtained in no-load conditions using analytical equations only. The geometry is then refined through a limited number of FEM simulations to satisfy the rated load performances.

In the paper, the proposed sizing methodology is validated considering as case study a reversely engineered salient-pole wound field synchronous motor used for traction applications. In particular, the electromagnetic information retrieved on the real machine has been used as input for the sizing code, obtaining a lamination that well matches the reference WFSM.

TABLE I. DESIGN INPUT DATA

| Design targets | Maximum electromagnetic loading limits | Geometrical and winding specifications |
|---|---|---|
| Torque ($T$) | Air-gap flux density at no-load ($B_{g,max}$) | Machine aspect ratio ($\lambda=L/D_g$) |
| Speed ($n$) | Stator yoke flux density at no-load ($B_{sy,max}$) | Pole pairs number ($p$) |
| Stator phase voltage ($V_s$) | Rotor yoke flux density at no-load ($B_{ry,max}$) | Number of slots per pole per phase ($q$) |
| Rotor voltage ($V_r$) | Teeth flux density at no-load ($B_{t,max}$) | Minimum inner diameter ($D_{ri}$) |
| Operating temperature ($\theta$) | Rotor pole flux density at no-load ($B_{p,max}$) | Air gap thickness ($g_0$) |
| Power factor, ($cos(\varphi)$) | Stator current density ($J_{s,max}$) | Slot opening dimensions ($h_1$, $h_2$, $w_0$) |
| Target efficiency ($\eta$) | Rotor current density ($J_{r,max}$) | Stator and rotor slot filling coefficient ($k_{fs}$, $k_{fr}$) |
| Lamination BH-curve and stacking factor $k_{st}$ | Linear current density ($A_{s,max}$) | Pole span ($k_b$) |

## II. PROCEDURE INPUTS AND ASSUMPTIONS

The input data of the electromagnetic sizing algorithm comprehend the desired rated performances, the admissible electromagnetic loadings, some geometrical specifications, and a basic winding layout. Table I lists all the requested input data.

The rated electromagnetic torque represents the target of the sizing algorithm, while the stator and rotor voltages are input data that must be chosen accordingly to the available power source. For what it concerns the electromagnetic loadings (rotor and stator current density, linear current density, and magnetic flux densities), their maximum allowed values depend on the insulation and the cooling of the machine. Empirically defined variation ranges of the electromagnetic loadings are well-known, and their typical values can also be found in textbooks. It is worth noting that large machines usually feature low (superficial) current densities. On the contrary, low values of the linear current density must be adopted for small machines [13].

Among the geometrical specifications, the machine aspect ratio $\lambda$ is defined as the ratio of the active core length ($L$) and the air gap diameter ($D_g$). Its value characterizes the shape of the machine and can be fixed according to the volume constraints dictated by the specific application. The minimum inner diameter is also fixed, depending on the mechanical layout as well as on the shaft diameter that is required to deliver the output torque. The number of poles is also an input for the developed sizing procedure since it must be chosen as a trade-off between the required rotational speed and the supply frequency. Similarly, the slot enclosure dimensions are also imposed by the user according to the winding construction process that is intended to be used.

In salient-pole WFSMs, the pole shoe is generally shaped such that the magnetic flux density at the air gap is proportional to the cosine of the electrical angle $p\theta$, being $\theta$ the mechanical angle shown in Fig. 1 [13], [14]. Thus, the air gap length varies as in (1), where $g_0$ is the minimum air gap thickness in correspondence of the middle of the rotor pole ($g_0=(D_{si}-D_{ro})/2$).

$$g(\theta)=\frac{g_0}{\cos(p\cdot\theta)} \qquad for \quad 0\le\theta\le\frac{\pi}{2p} \tag{1}$$

In the proposed sizing code, the value of $g_0$ is set as an input. Theoretically, its value should be as small as feasible to minimize the magnetizing current.

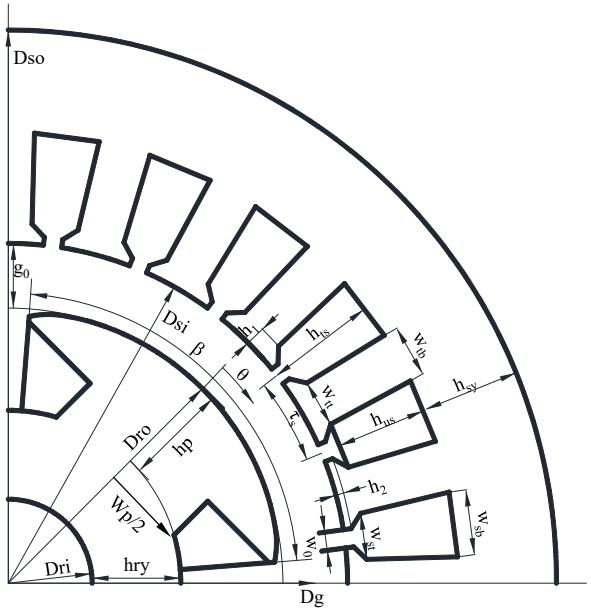


Fig. 1 Sketch of the cross section of WFSM.

Nevertheless, smaller air gaps produce larger eddy current losses because of the permeance harmonics of the slot openings. According to [13], in synchronous machines, the minimum value of the air gap length can be found by imposing the rotor ampere-turns to be higher than the armature ampere-turns, with the aim of limiting the armature reaction. Its formulation is reported in (2), where γ is a coefficient that depends on the type of the machine (for the salient pole WFSM, its value is $7\cdot10^{-7}$), $\tau_p$ is the pole pitch at the air gap, $A_s$ is the stator current density and $B_g$ is the air gap magnetic flux density.

$$g_0 \ge \gamma\cdot\tau_p\cdot\frac{A_s}{B_g} \tag{2}$$

Finally, the pole shoe width as percentage of the pole pitch, $k_b$, is defined by (3). Higher values of $k_b$ mean lower values of the saliency ratio; in this case the resulting geometry features a better mechanical enclosure of the rotor conductors, but also a larger leakage flux among the poles.

$$k_b=\frac{\beta}{\pi/p} \tag{3}$$

## III. Sizing Procedure and Algorithm

The proposed electromagnetic sizing procedure has been implemented in Matlab®. However, any programming language or numerical computing language can be used for this purpose. The algorithm follows the flow chart in Fig. 2 and pursues the two subsequent steps described hereafter.

### *A. Preliminary lamination design in no-load conditions*

At this stage a preliminary lamination geometry is created only relying on analytical equations and considering the machine magnetic loadings in no-load operation. The sizing process starts by computing the main machine's dimensions, imposing an initial air gap diameter that is slightly greater than the constrained minimum inner rotor diameter. Therefore, the value of the flux per pole is computed on the basis of the imposed maximum air gap flux density as in (4), where $L$ is the machine core length.

$$\Phi = \alpha_s \cdot \tau_p \cdot L \cdot B_{g,max} \tag{4}$$

The parameter $\alpha_s$ is the coefficient of the arithmetical average of the magnetic flux density, which is equal to $2/\pi$ for a sinusoidal distribution. However, when the lamination saturates, the air gap flux density is distorted, affecting the value of $\alpha_s$. Therefore, in the developed sizing procedure, the correct value of $\alpha_s$ is iteratively determined once the geometric dimensions are defined.

The number of turns in series per phase is determined as in (5), where $k_w$ is the winding factor, $f$ is the electrical frequency, and $E$ is the electromotive force. Considering the impact of the armature reaction, it is assumed that the value of the no-load voltage $E$ might exceed of 1.2-1.3 times the stator voltage $V_s$ in load conditions. Such a range is considered reasonable also for high armature reaction machines [13].

$$N_s = \frac{E}{2\pi/\sqrt{2} \cdot k_w \cdot f \cdot \Phi} \tag{5}$$

The value of the stator current is obtained considering the needed active power, knowing the imposed stator voltage, the speed, the efficiency, and the power factor, as expressed in (6).

$$3 \cdot V_s \cdot I_s \cdot \eta \cdot \cos(\varphi) = T \cdot n \cdot \frac{\pi}{30} \tag{6}$$

Hence, the value of the stator linear current density (7) is computed, where $N_{ss}$ is the number of stator slots.

$$A_s = \frac{I_s \cdot m \cdot 2N_{ss}}{\pi D_g} \tag{7}$$

If the resulting current density exceeds the corresponding imposed constraint, the air gap diameter is increased of a defined step size $\Delta D_g$, and the computation is repeated. Once the loop is solved, the main dimensions of the lamination geometry are obtained.

The remaining geometrical variables are found on the basis of the resulting flux per pole. In detail, the tooth width $w_{tt}$ is computed by (8), considering the magnetic flux related to one slot pitch $\tau_s$.

$$\tau_s \cdot L \cdot B_{g,max} = w_{tt} \cdot L \cdot k_{st} \cdot B_{t,max} \tag{8}$$

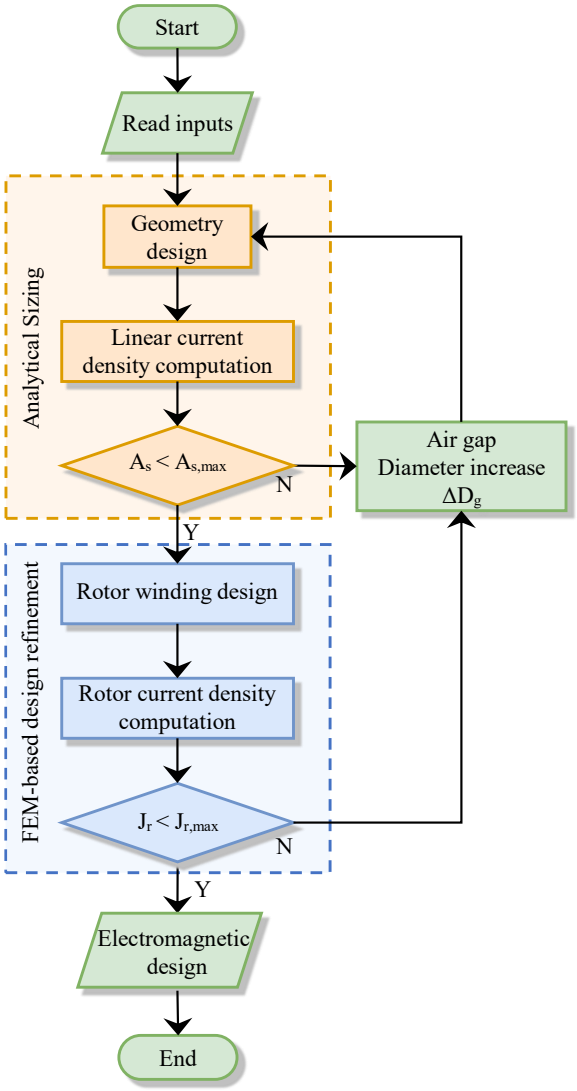


Fig. 2 Algoritm flow-chart of the proposed sizing procedure.

The stator slot area is determined by the stator current density $J_s$ and the linear current density, as in (9).

$$S_s = \frac{A_s \cdot \tau_s}{k_{fs} \cdot J_s} \tag{9}$$

Therefore, the stator slot height can be simply determined by geometrical considerations, depending on the desired slot shape. Taking into account that the developed code is intended for a fast lamination sizing, only simple slot geometries, such as rectangular or trapezoidal shapes, have been considered. Further detailed refinements, such as fillets or particular slot shapes, can then be addressed in the project finalization stage without heavily impacting the machine performance [15], [16].

Once the tooth dimensions have been defined, the value of $\alpha_s$ is updated on the basis of the ratio between the teeth magnetic voltage and the air gap magnetic voltage, as explained in [13]. Therefore, a new value for the air gap flux density is computed by (4) and the lamination design updated. The process is iteratively repeated until the convergence on $\alpha_s$ is achieved with a defined tolerance.

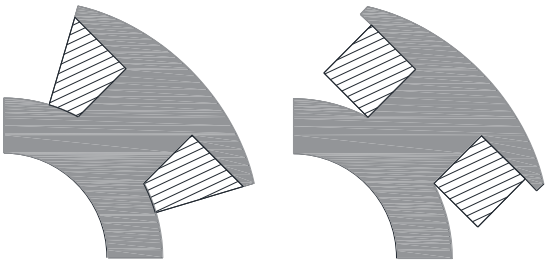

Fig. 3 Rotor slot geometries considered in the developed sizing code.

The width of the rotor yoke, rotor pole and stator yoke are obtained by solving the magnetic circuit in the *d*-axis for the magnetic flux computed by (3). For what it concerns the rotor '*slot*' area, it is computed according to the selected rotor slot geometry. For the developed code the two alternatives shown in Fig. 3 have been implemented.

### *B. Lamination design in load conditions*

The second part of the sizing process is pursued in load conditions, determining the stator and rotor currents that guarantee the desired rated performances. In fact, despite the magnitude of the stator current vector has already been defined through (6), its orientation in the *dq* reference frame associated to a rotor-flux-oriented coordinate system is still unknown. Moreover, also the rotor ampere-turns $N_r I_r$, and ultimately the rotor current, must be determined with the aim of providing the required machine magnetization. Furthermore, by (6) it is also clear that the desired torque must be obtained respecting both the imposed stator voltage $V_s$ and the power factor.

For this purpose, the developed algorithm links Matlab® to the finite element software FEMM [17]. As shown in Fig. 4, finite element simulations are run for different values of the stator current vector angle $\Psi$ and for different values of the rotor ampere-turns. In detail, the geometry obtained from the preliminary analytical design is built in the finite element software and a grid of different combinations of $\Psi$ and $N_r I_r$, as shown in Fig. 5a, is simulated for one magnetic periodicity of the machine [18], [19]. It is worth noticing that, for high power factor values the investigation range for the stator current vector can be limited to the second quadrant of the *dq*-frame [20]. For the rotor ampere-turns, the investigation range is set according to the ampere-turns computed for the no-load operation. For each rotor position, the $\lambda_d$ and $\lambda_q$ linked magnetic fluxes are computed and then averaged over all the simulated rotor positions. From the magnetic flux values, the *d*- and *q*-axis voltages are obtained as in (10).

$$\begin{cases} v_d = -\omega\lambda_q \\ v_q = \omega\lambda_q \end{cases} \tag{10}$$

Thus, for each point of the simulation grid in Fig. 5a, it is possible to compute the magnitude and phase of the stator voltage vector, and the power factor. Among all the simulated points, the sizing algorithm identifies the pair of $\Psi$ and $N_r I_r$ values that satisfies the imposed $V_s$ and $\cos(\varphi)$ for the specific load condition. As an example, Fig. 5b, shows the resulting phasor diagram for a unitary power factor. Once the rotor ampere-turns at load have been determined, the value of the rotor turns is obtained by applying the Ohm law:

$$N_r = \frac{V_r \cdot S_r \cdot k_{fr}}{2p \cdot \rho \cdot L \cdot (N_r I_r)} \tag{11}$$

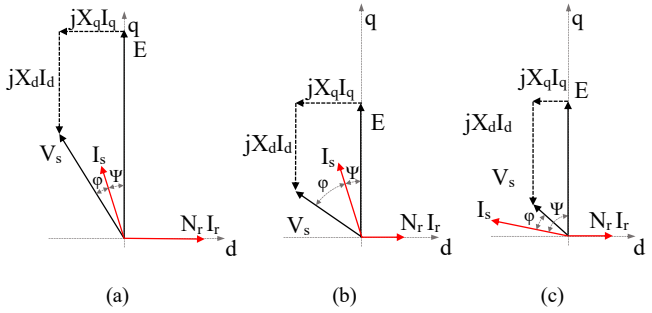


Fig. 4 The phasor diagram with negligible stator resistance changing the angle of the stator current (a)-(b) or the rotor ampere-turns (b)-(c).

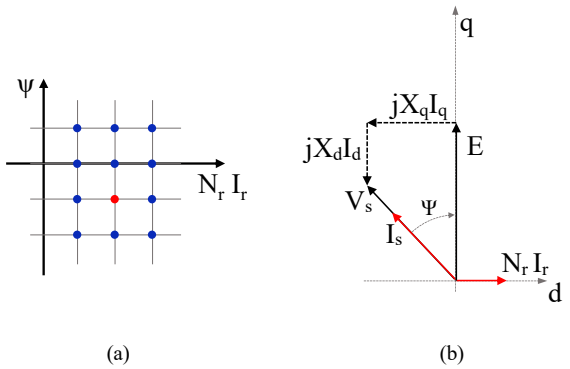


Fig. 5 Grid of the performed FEM simulations (a) and phasor diagram (b) for the target load condition with unitary power factor (red point in the grid).

In (11), $S_r$ is the rotor *'slot'* area, while $\rho$ is the copper resistivity at the specified operating temperature. The rotor current is obtained by dividing the ampere-turns by the number of rotor turns. Finally, the value of the rotor current density can be easily computed by (12).

$$J_r = \frac{N_r I_r}{S_r \cdot k_{fr}} \tag{12}$$

The rotor current density is thus compared to its maximum value set as input. If the obtained value exceeds the limit, as depicted in Fig. 2, the air gap diameter is again increased of the step size $\Delta D_g$ and the computation is repeated; otherwise, the algorithm is ended, and the machine sizing completed.

## IV. Sizing Procedure Validation

Several random WFSMs have been sized and simulated in FEM to test that the proposed procedure always reaches the desired performances by respecting all the imposed constraints. However, in order to prove that the machine volume obtained by the code has a valid correspondence with existing machines, this paper validates the sizing procedure considering as case study a highly engineered WFSM used for traction applications.

### *A. The WFSM for the sizing procedure validation*

The considered machine under rated performances is a 51 kW, 3-phase, 4-poles motor with a base speed of 4000 rpm and supplied by a 400V dc-link [21]. The lamination geometry and materials, as well as the winding layout have been reversely engineered by the authors on the sample shown in Fig. 6.

In order to retrieve the magnetic and electric permissible limits that need to be set as input for the proposed sizing code, the machine has been analyzed through FEM simulations. The values of the maximum magnetic loadings in the machine core have been found in no-load conditions, imposing a rotor current such that the induced voltage at the stator terminals was compatible with the voltage levels of the dc-link. In these operative conditions, the amplitude of the fundamental component of the air gap flux density resulted equal to 0.9 T, that sounds as a reasonable value.

To define the stator and rotor current values to perform load simulations, it must be considered that the rated machine torque can be obtained for different combinations of the rotor current and the *dq*-stator currents, depending on the adopted control strategy. For this purpose, the current-to-flux linkage model for different rotor currents has been determined, as shown in Fig. 7. Nevertheless, the selection of the most appropriate control strategy for this machine is beyond the scope of this paper. Among all the possible alternatives, the rotor and stator current combination that maximize the machine power factor has been selected [22].

The stator and rotor current densities are computed by (13) and (14), where $S_{cu,s}$ and $S_{cu,r}$ are the measured conductor areas, while $a$ are the number of external and internal parallels paths of the stator winding.

$$J_{s,max} = \frac{I_s}{a \cdot S_{cu,s}} \tag{13}$$

$$J_{r,max} = \frac{I_r}{S_{cu,r}} \tag{14}$$

Similarly, the slot filling factors have been computed by the geometrical quantities measured on the machine under consideration. For what it concerns the value of the machine efficiency in (6), it has been estimated considering the stator and rotor Joule losses and by computing the iron losses through the FEM simulations, while friction and windage losses have been neglected for this preliminary machine sizing at the base speed.

Table II lists all the electromagnetic loading limits imposed as input for the sizing procedure for the WFSM considered as case study for the code validation.

### *B. The sized wound field synchronous motor*

The retrieved design targets, electromagnetic loadings and geometrical and winding information are used as input of the proposed sizing algorithm. The second part of the algorithm was set to simulate 10x10 combinations of rotor ampere-turns and stator current vector angle for each machine design. The overall procedure took less than one hour in a PC with 16 GB RAM and a parallelization over 8 cores.

Figure 8a depicts the colour-shaded map of the magnetic flux density at no-load conditions and with a fundamental maximum value of the air gap flux density of 0.9T. The tags in the figure show the maximum values achieved in the different machine parts, that well match with those set as input for the sizing procedure (see Table II). Figure 8b shows the obtained phasor diagram of stator voltage and current at load, and the induced voltage at no-load.

Fig. 6 WFSM motor and its rotor.

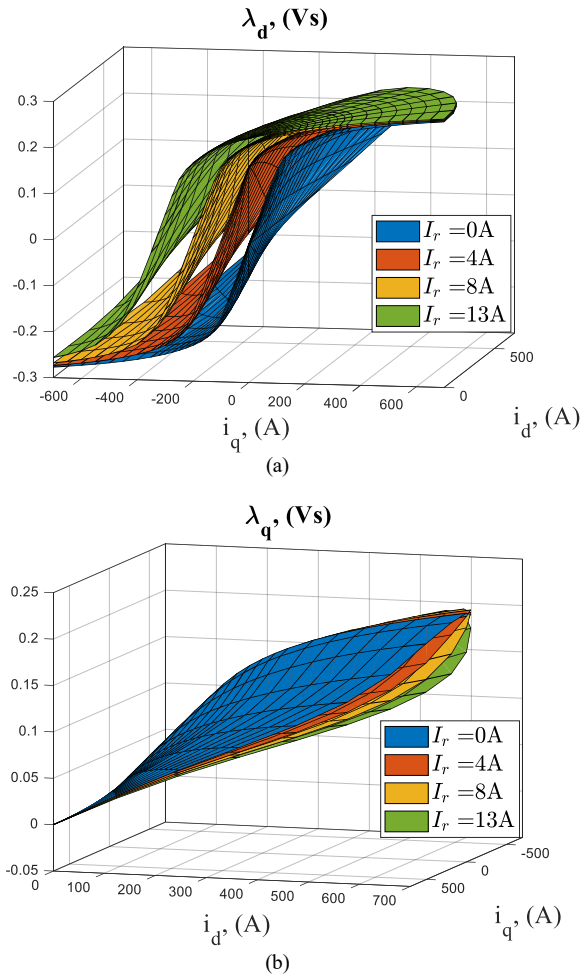


Fig. 7 Current-to-flux linkage model for the WFSM considered for the sizing code validation.

TABLE II. ELECTROMAGNETIC LOADING LIMITS FOR THE CASE STUDY

| | |
|---|---|
| Stator linear current density ($A_{s,max}$) | 385 A/cm |
| Stator current density ($J_{s,max}$) | 7 A/mm$^2$ |
| Rotor current density ($J_{r,max}$) | 8 A/ mm$^2$ |
| Air-gap flux density at no-load ($B_{g,max}$) | 0.9 T |
| Stator yoke flux density at no-load ($B_{sy,max}$) | 1.5 T |
| Rotor yoke flux density at no-load ($B_{ry,max}$) | 1.5 T |
| Teeth flux density at no-load ($B_{t,max}$) | 1.7 T |
| Rotor pole flux density at no-load ($B_{p,max}$) | 1.7 T |

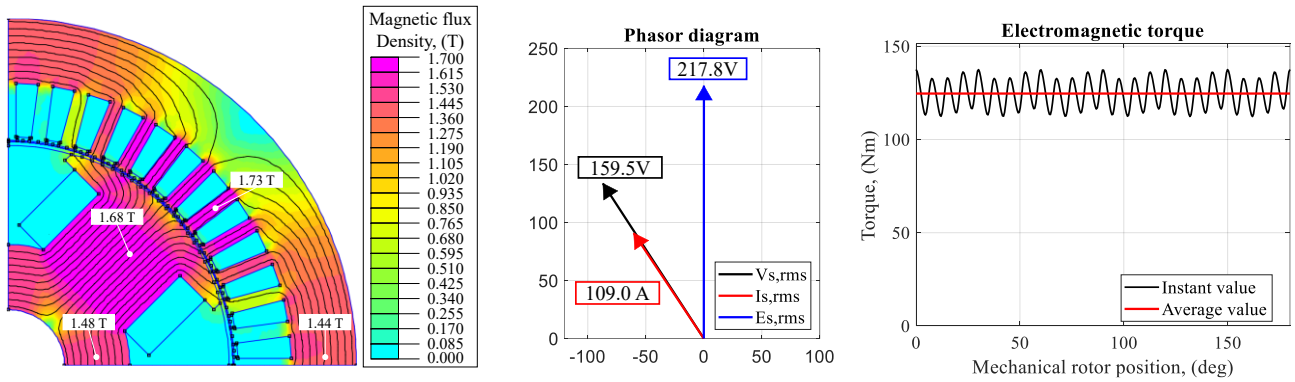


(a) (b) (c)

Fig. 8 Colour shaded map of no-load flux density (a), phasor diagram (b), and electromagnetic torque (c).

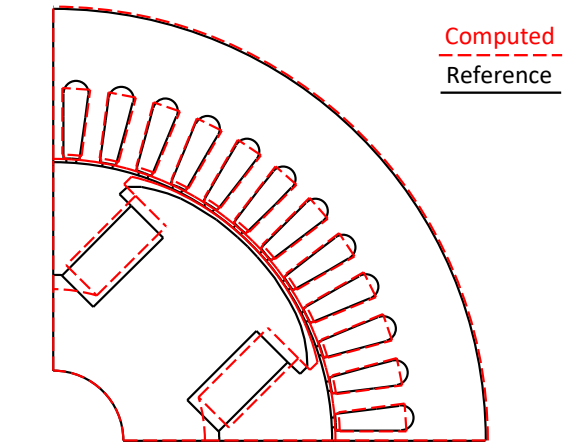


Fig.9 Comparison between the sized and the reference geometry.

The obtained stator voltage is 159.5 V (being 160 V the stator voltage input) with a unitary power factor, as requested by the inputs of the algorithm. The resulting average electromagnetic torque, in Fig. 8c, is 124.7 Nm, meaning an error of 3.9 % with respect to the requested value of 120 Nm. However, it must be highlighted that the value obtained by the finite element software is an electromagnetic torque that does not consider the selected input value of the efficiency.

Figure 9 overlaps the obtained geometry (red dotted lines) with the reference WFSM, and minor differences can be seen between the two lamination geometries. To be more specific, Table III reports the comparison of the main geometric variables, whose names are defined in Fig. 1. Note that the larger percentage errors have been obtained for the stator and rotor yoke thicknesses. However, as evident in Fig. 9, such dimensions are strongly affected by the real shape of the stator and rotor slots to accommodate the conductors, that are not accounted in the proposed design procedure. Thus, also in this case, the obtained results are considered well acceptable.

The resulting performances are reached while respecting all the constraints, and in particular the obtained value of the stator linear current density is 372 A/cm, while the rotor current density is 7.95 A/mm$^2$. All the other inputs are not used as check conditions, but as input parameters, thus the obtained values are exactly the requested ones.

TABLE III. GEOMETRIC COMPARISON OF THE COMPUTED WFSM WITH THE REFERENCE

| Geometric variable | Computed (mm) | Reference (mm) | Error (%) |
|---|---|---|---|
| $L$ | 176.5 | 174.4 | 1.2 % |
| $D_{so}$ | 243.3 | 242.2 | 0.5 % |
| $D_g$ | 157.1 | 155.6 | 1.0 % |
| $h_{sy}$ | 22.8 | 21.3 | 7.0 % |
| $h_p$ | 35.6 | 37.8 | -5.8 % |
| $h_{ry}$ | 22.8 | 19.6 | 16.3 % |
| $w_{tt}$ | 5.1 | 5.2 | -1.9 % |
| $w_p$ | 40 | 37.7 | 6.1 % |

## V. CONCLUSION

This paper proposes an electromagnetic sizing procedure for fast sizing of salient-pole WFSMs. The procedure is based on an analytical-numerical approach consisting of the progressive growth of the machine dimensions until all the imposed inputs are satisfied. A first lamination geometry is obtained by analytical equations in no-load conditions, while FEM simulations allow defining the final machine geometry that satisfies the design targets and constraints.

The procedure has been validated reversely engineering a highly engineered traction motor, using the retrieved information as input of the sizing code. Results show that the obtained lamination dimensions are in good agreement with those of a reference machine, while achieving the same performances. The authors intend to further develop the proposed procedure including both thermal and mechanical verifications, still maintaining the nature of a preliminary design tool to be subjected to refinements for the project finalization.

## REFERENCES

[1] H. -J. Park and M. -S. Lim, "Design of High Power Density and High Efficiency Wound-Field Synchronous Motor for Electric Vehicle Traction," in *IEEE Access*, vol. 7, 2019.

[2] N. Tang, D. Sossong and I. P. Brown, "Design and Metamodel-Based Optimization of a High Power Density Wound Field Traction Motor," 2021 IEEE Energy Conversion Congress and Expo (ECCE), 2021.

[3] D. G. Dorrell, "Are wound-rotor synchronous motors suitable for use in high efficiency torque-dense automotive drives?," IECON 2012 - 38th Annual Conference on IEEE Industrial Electronics Society, 2012.

[4] F. Graffeo, S. Vaschetto, M. Cossale, M. Kerschbaumer, E. C. Bortoni,A. Cavagnino, "Cylindrical Wound-Rotor Synchronous Machines for Traction Applications," 2020 International Conference on Electrical Machines (ICEM), 2020, pp. 1736-1742.
[5] C. Rossi, D. Casadei, A. Pilati and M. Marano, "Wound Rotor Salient Pole Synchronous Machine Drive for Electric Traction," Conference Record of the 2006 IEEE Industry Applications Conference Forty-First IAS Annual Meeting, Tampa, FL, USA, 2006, pp. 1235-1241.
[6] A. Di Gioia, I. P. Brown, Y. Nie, R. Knippel, D. C. Ludois, et al., "Design and Demonstration of a Wound Field Synchronous Machine for Electric Vehicle Traction With Brushless Capacitive Field Excitation," in *IEEE Trans. Ind. Appl.*, vol. 54, no. 2, 2018.
[7] Bazzo, T.d.P.M.; Moura, V.d.O.; Carlson, R. A Step-by-Step Procedure to Perform Preliminary Designs of Salient-Pole Synchronous Generators. Energies 2021, 14, 4989.
[8] N. Tang and I. P. Brown, "Comparison of Candidate Designs and Performance Optimization for an Electric Traction Motor Targeting 50 kW/L Power Density," 2021 IEEE Energy Conversion Congress and Exposition (ECCE), Vancouver, BC, Canada, 2021.
[9] S. Udema and C. Fraeger, "Design of a Highly Efficient Electrical Excited Salient-Pole Synchronous Machine Utilizing an Optimization Algorithm," Innovative Small Drives and Micro-Motor Systems; 11th GMM/ETG-Symposium, Saarbruecken, Germany, 2017.
[10] O. Laldin, S. D. Sudhoff and S. D. Pekarek, "An analytical design model for wound rotor synchronous machines," 2013 IEEE Electric Ship Technologies Symposium (ESTS), Arlington, VA, USA, 2013.
[11] J. -J. Lee, J. Lee and K. -S. Kim, "Design of a WFSM for an Electric Vehicle Based on a Nonlinear Magnetic Equivalent Circuit," in IEEE *Trans. Appl. Superconductivity*, vol. 28, no. 3, pp. 1-4, April 2018.
[12] M. G. Pasquinelli, P. Bolognesi, A. Guiducci, S. Nuzzo and M. Galea, "Design of a High-Speed Wound-Field Synchronous Generator for the More Electric Aircraft," 2021 IEEE Workshop on Electrical Machines Design, Control and Diagnosis (WEMDCD), Modena, Italy, 2021.
[13] J. Pyrhonen, T. Jokinen, V. Hrabovcova, "Design of Rotating Electrical Machines", 2nd edition, Wiley, 2014.
[14] M. Biasion, D. Kowal, R. R. Moghaddam and M. Pastorelli, "Influence of the Lamination Material and Rotor Pole Geometry on the Performance of Wound Field Synchronous Machines," 2022 IEEE Energy Conversion Congress and Exposition (ECCE), 2022.
[15] A. Boglietti, A. Cavagnino, M. Lazzari, S. Vaschetto, "Preliminary induction motor electromagnetic sizing based on a geometrical approach," 2012 Electric Power Applications, IET. 6. 583-592. 10.1049/iet-epa.2012.0037.
[16] S. Vaschetto, A. Tenconi and G. Bramerdorfer, "Sizing procedure of surface mounted PM machines for fast analytical evaluations," 2017 IEEE Int. Electric Machines and Drives Conference (IEMDC), 2017.
[17] David Meeker, Finite Element Method Magnetics (FEMM). [Online]: https://www.femm.info/wiki/HomePage (accessed Mar. 29, 2023)
[18] S. Ferrari, G. Dilevrano, P. Ragazzo and G. Pellegrino, "The dq-theta Flux Map Model of Synchronous Machines," 2021 IEEE Energy Conversion Congress and Exposition (ECCE), 2021, pp. 3716-3723.
[19] R. Bojoi, A. Cavagnino, M. Cossale and S. Vaschetto, "Methodology for the IPM motor magnetic model computation based on finite element analysis," IECON 2014 - 40th Annual Conference of the IEEE Industrial Electronics Society, Dallas, TX, USA, 2014, pp. 722-728.
[20] D. Hwang and B. -G. Gu, "Field Current Control Strategy for Wound-Rotor Synchronous Motors Considering Coupled Stator Flux Linkage," in IEEE Access, vol. 8, 2020.
[21] [Online]: https://de.wikipedia.org/wiki/Renault_Zoe (Mar. 29, 2023).
[22] C. Szabo, M. Imecs and I. I. Incze, "Double-field orientation of unity power factor synchronous motor drive," 2010 IEEE 14th Int. Conf. on Intelligent Engineering Systems, Las Palmas, Spain, 2010.

## ACKNOWLEDGMENT

This study was carried out within the MOST – Sustainable Mobility National Research Center and received funding from the European Union Next-GenerationEU (PIANO NAZIONALE DI RIPRESA E RESILIENZA (PNRR) – MISSIONE 4 COMPONENTE 2, INVESTIMENTO 1.4 – D.D. 1033 17/06/2022, CN00000023). This manuscript reflects only the authors' views and opinions, neither the European Union nor the European Commission can be considered responsible for them.

## BIOGRAPHIES

**Federica Graffeo** (S'20) received the B.Sc. degree in Energy Engineering from Università degli Studi di Palermo (Italy) and the M.Sc. degree in Electrical Engineering from Politecnico di Torino (Italy) in 2017 and 2020, respectively. She is currently working toward the Ph.D. degree at the Department of Energy, Politecnico di Torino. Her research interests include electromagnetic and thermal design of synchronous electrical machines for transportation applications.

**Silvio Vaschetto** (S'10–M'13–SM'19) received the M.Sc. and Ph.D. degrees in electrical engineering from the Politecnico di Torino, Italy, in 2007 and 2011, respectively. He then joined ABB IEC LV Motors Technology Center, Vittuone, Italy as R&D engineer. From 2012 to 2014 he was with Magna Electronics Italy, as Electromagnetic Simulation and Motor Design Engineer. He is currently an Associate Professor at the Energy Department "G. Ferraris", Politecnico di Torino. His research interests include electromagnetic design, thermal design, and energetic behavior of electrical machines for high-performance applications. He is an Associate Editor for IEEE TRANSACTIONS ON INDUSTRY APPLICATIONS and for IET Electric Power Applications.

**Alberto Tenconi** (M'99–SM'10) received the M.Sc. and Ph.D. degrees in electrical engineering from the Politecnico di Torino, Torino, Italy, in 1986 and 1990, respectively. From 1988 to 1993, he was with the Electronic System Division, FIAT Research Center, where he was engaged in the development of electrical vehicle drive systems. He then joined the Department of Electrical Engineering (now Energy Department), Politecnico di Torino, where he is currently full professor. His research activity is documented by more than 200 papers published in International Journals and International Conferences. He has participated, both as a designer and as scientific responsible, in many National and European Research Programmes. He is a reviewer for International Journals and has been Associate Editor for the Transactions on Industrial Electronics. His current research interests include electric machines, power converters and drives for transportation electrification.

**Andrea Cavagnino** (M'04–SM'10–F'20) received his Ph.D. degree in electrical engineering from the Politecnico di Torino, Italy, in 2000 where he is a professor on electrical machine and drives. His research interests include electromagnetic design, thermal design, and energetic behaviour of electrical machines. He usually cooperates with factories for a direct technological transfer and he has been involved in several public and private research projects. He has authored or co-authored more than 250 papers, receiving four Best Paper Awards. Prof. Cavagnino is an Associate Editor of the IEEE TRANSACTIONS ON ENERGY CONVERSION and he was a technical program chair of the IEEE-IEMDC 2015 and IEEE-ECCE 2022 conferences.